AlGaAsSb/InGaAsSb photovoltaic transistors and high efficient solar cell with nano-antenna structures

Chunchen Lin, Nikolai Faleev, and Dennis Prather
Department of Electrical and Computer Engineering, University of Delaware, Newark DE USA 19716

ABSTRACT

We present a new design of high sensitivity, multi-spectral capability AlGaAsSb/InGaAsSb phototransistors for infrared sensing and solar energy conversion applications. These devices are grown by molecular beam epitaxy (MBE), which exhibit high responsivity at room-temperature. The 50% cutoff wavelength of spectral photoresponse is 2.2 µm. Similar structures are also investigated for solar cell applications. The possibility of increasing the solar energy conversion is explored by incorporating nano-antenna array into the solar cell. The broad-band nano-antenna is designed using Ansoft HFSS. The results indicate high solar energy conversion can be achieved for highly efficiency, flexible, lightweight solar power generations for the applications such as aircraft, airbase and special operations

Keywords: Photo transistor, antenna solar cell, detector

1. INTRODUCTION

Infrared (IR) detectors have unique applications in atmospheric remote sensing, optical communications, and absorption spectroscopy. In particular, the spectral range 2.0–2.4 µm wavelength is of great interest for several special applications including profiling of atmospheric CO_2 using light detection and ranging (LIDAR) techniques, non-invasive monitoring of blood glucose using absorption spectroscopy. Although InGaAs and HgCdTe detectors can be used for this purpose, they lack sufficient responsivity due to the absence of internal-gain mechanisms. Besides, in the IR wavelength, these detectors operate in the low temperature, which increases the system complexity. InGaAsSb quaternary material shows promising performance for IR detectors [1]. On the other hand, heterojunction phototransistors (HPTs) have attracted considerable attention recently as a promising alternative to p-i-n photodiodes or avalanche photodiodes, because it can provide a large spectral responsivity without a high bias voltage and excess avalanche noise. Developments of heterojunction n-p-n and p-n-p phototransistors (HPTs) using InGaAsSb/AlGaAsSb material were reported [1-2]. The advantage of these HPTs is their optimization around the 2 µm wavelength with high internal gain, which leads to high responsivity and high SNR.

Both n-p-n and p-n-p type HPTs based on the InGaAsSb material system have been reported by different groups [1]-[2]. The reported devices exhibited excellent performances at room temperature for the wavelength range around and above 2.0 µm. High optical gains were achieved for both n-p-n and p-n-p AlGaAsSb–InGaAsSb HPT structures. For the n-p-n heterojunction structure, the highest gain reported is grown by liquid phase epitaxy (LPE) method. Although the LPE-related work resulted in the fabrication of an HPT with excellent parameters, the room temperature cutoff wavelength of these devices was determined by fundamental limitations implied by the close-to equilibrium growth from Al-In-Ga-As-Sb melts. Alternative methods include Molecular-beam epitaxy (MBE) or metal oxide chemical vapor deposition (MOCVD) method. MBE provides provides better control over doping levels, composition and width of the AlGaAsSb and InGaAsSb layers, compositional and doping profiles, especially with regard to abrupt heterojunctions. Therefore, devices with longer cutoff wavelengths could be fabricated. On the other hand, metal MOCVD provides better lattice match and therefore, less crystalline imperfection, which results in low dark current.

In this paper, both n-p-n and p-n-p AlGaAsSb-InGaAsSb phototransistor structures fabricated with MBE and MOCVD grown heterojunction structures are presented. The related results are compared and analyzed to select the high quality devices with high gain and low dark current. In addition, devices with the optical gain of 3000 were fabricated and characterized. Room-temperature spectral photoresponse is obtained with a 50% cutoff wavelength at 2.2 µm.

Optical Components and Materials V, edited by Michel J. F. Digonnet, Shibin Jiang, John W. Glesener, J. Christopher Dries
Proc. of SPIE Vol. 6890, 68900D, (2008) · 0277-786X/08/$18 · doi: 10.1117/12.763847

In particular, the current density of the photodetector is much higher than currently solar cell, which triggers us to purpose a high efficient solar cell based on the detector. Solar energy conversion is a potential alternative for traditional power sources. The low efficiency of conversion solar energy into electricity is the key issue in solar cell applications. The high gain of the InGaAsSb/AlGaAsSb photo detector can be used to compliment the low efficiency of the solar cell in infrared regime. In addition, antennas, which collect power from passing electromagnetic waves, have been developed since the very beginning of electromagnetism. By incorporating antenna into solar cell, the conversion efficiency is expected to be significantly increased by collecting more solar radiation. Although antenna has broad applications in radio frequency and microwave regime of electromagnetic spectrum, optical antenna has not been purposed and demonstrated until recently due to the fabrication limitation in the shorter wavelength.

Antenna working in the optical regime became available with the development of electron beam lithography and similar techniques with sub-micron resolution [3]. In addition, in optical wavelength, the dimension of the optical antenna reaches the length of excitation of surface plasmons (SPs). If the wavelength is suitably matched to the size of the resonant antenna, the electromagnetic field can be significantly enhanced and localized. In this paper, we will present our simulation results of designed wide band bowtie antenna for solar cell application using Ansoft HFSS. The bandwidth of the antenna covered most part of the solar spectrum from 300 nm to 750 nm. The effect of the parameters of the antenna, such as the width of the gap, the length, and the angle of the antenna to the bandwidth and field enhancement is discussed. To further explore the feasibility of the antenna.

2. HPTS DEVICE CHARACTERIZATIONS

The HPT is two terminal devices with a floating base. Base current is generated optically through the incident light. The device is designed with a p-type (4×10^{17}cm^{-3}) 0.3-μm-thick $Al_{0.4}Ga_{0.6}As_{0.14}Sb_{0.86}$ emitter, and a 1.5 μm p-type (6×10^{16}cm^{-3}), $In_{0.16}Ga_{0.84}As_{0.14}Sb_{0.86}$ collector. The base is consisted of a 0.2 μm $Al_{0.4}Ga_{0.6}As_{0.14}Sb_{0.86}$ and a 0.5-μm $In_{0.16}Ga_{0.84}As_{0.14}Sb_{0.86}$ doped to n-type (6×10^{16}cm^{-3}). Heavily doped p-type (5×10^{17}cm^{-3}) GaSb layers are added at both ends for the emitter and collector contacts. The HPTs were defined using photolighography and wet chemical etching. Gold was evaporated on both front and back side of the device by electron-beam evaporation to form Ohmic contacts for the emitter and collector. A polyimide PI-2723 manufactured by HD Microsystems was spun on the front surface of the device to serve as planarization of the top surface, mesa isolation, and edge passivation.

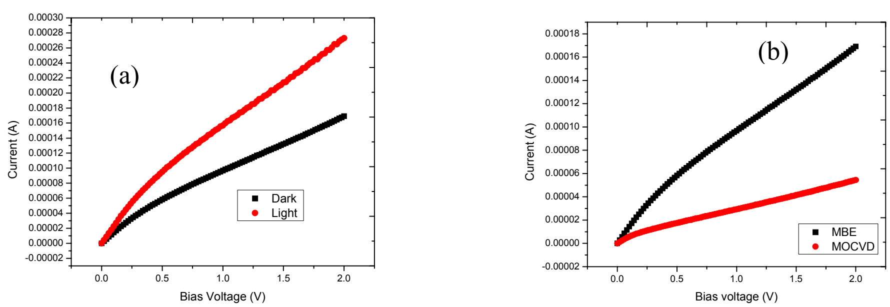

Fig. 1. (a) I-V measurement of the dark-current and the current under light illumination with different bias voltages of the p-n-p HPT grown by MBE technique, (b) Dark current of the MBE and MOCVD grown devices.

The fabricated devices are characterized for performance. Figure 1(a) shows the I-V characteristics of the phototransistors p-n-p type HPT grown by MBE technique under dark condition and infrared illuminations at 20 ◦C. The currents were measured using a semiconductor-characterization system under dark and light condition. As can be seen in Fig. 1, the device shows stable and high sensitivities above the knee voltage of 0.3 V. Figure 1 (b) shows the dark current of the MBE and MOCVD grown p-n-p HPTs. The dark current of the MBE grown device is higher than the MOCVD grown HPT. At the biased voltage of 2.0 V, the dark current of the MBE grown device is 0.18 mA, while the dark current of the MOCVD grown device is 0.03 mA. This because of the crystalline dislocation in the MBE grown devices is much higher than the MOCVD grown devices. This is confirmed by the XRD spectrum measurement of both MBE and MOCVD based devices as shown in Fig. 2. It shows the threading dislocations, which are the main crystalline defects in InGaAsSb layer and substrate in MOCVD grown devices is two orders lower than the MBE grown device.

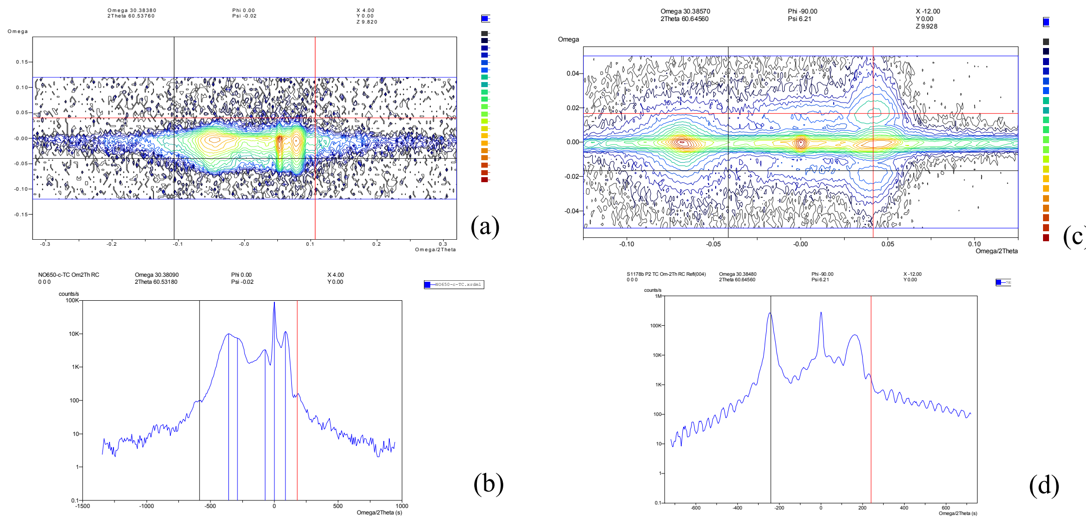

Fig. 2. (a) and (c) reciprocal Space Map, Refl(004) of MBE and MOCVD grown device layers, (b) and (d) HR ω-2θ and ω Rocking Curves of MBE and MOCVD grown device layers

The spectral response of the HPT was measured from 1.3-2.2 μm using an Oriel 77200 monochronometer. Fig. 3(a) and (b) show the spectral response of the p-n-p and n-p-n HPT detectors under zero and different bias voltages. For both p-n-p and n-p-n type HPTs, the spectral response cuts off around 2.2 μm with a spectral response ranging from 1000 to 2200 nm. For the p-n-p HPT, there are three peaks in the spectrum, which are at 1.38 μm, 1.79 μm and 2.17 μm, whereas, for the n-p-n HPT, there are at 1.22 μm, 1.68 μm and 2.16 μm, respectively.

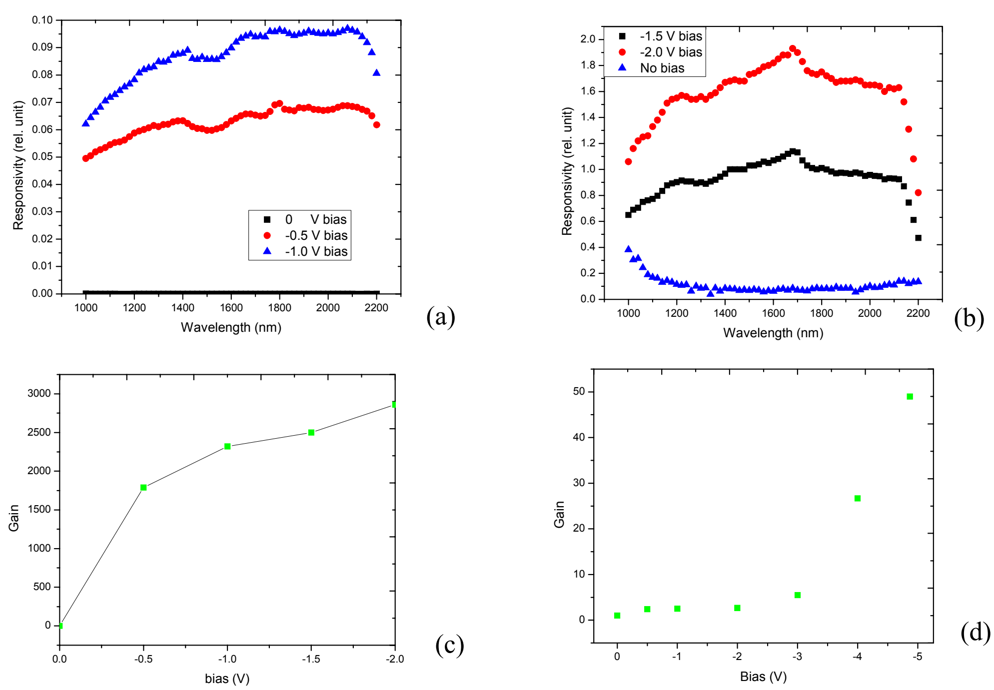

Fig. 3. (a) and (b) Spectral-response of MBE p-n-p and n-p-n HPTs, (c) and (d) Gain variation with the bias voltage of p-n-p and n-p-n HPTs.

There is a slight red-shift of the peaks for the n-p-n HPT comparing with the p-n-p HPT. For the p-n-p HPT, the responsivity increased significantly with the applied bias voltage, indicating high device gain. This prediction is confirmed by the gain calculation shown in Fig. 3 (c). The maxim gain of the p-n-p HPT reaches 3000.

The high gain of the p-n-p device comes from the conduction band offset between AlGaAsSb and InGaAsSb is much larger than the valence band offset [2]. During the operation of p-n-p AlGaAsSb-InGaAsSb phototransistor, the reverse injection of electrons from the InGaAsSb base region into the emitter is efficiently suppressed by the high conduction band offset at the emitter-base (E-B) interface [2].

3. ANTENNA SOLAR CELL SIMULATION

The current density of the p-n-p HPT is orders of magnitude higher than that of the current solar cell, shown in Fig. 4 (a). If it is used for solar cell application, it will increase the efficient of the solar energy conversion significantly in the infrared range of the solar spectrum. In this case, we incorporate nano-antenna into the structure to further increase the energy collection of the solar cell, as shown in Fig. 4(b). For the broadband application, the antenna is chosen as a bowtie antenna fabricated on a 50 nm thick silicon substrate with plane wave illumination introduced from the free space. A 5 nm gold ground plane is added to the other side of the substrate to enhance the field collection. The antenna is gold with finite conductivity of 1.28×10^7 with the length, width, and the gap size of 96 nm, 60 nm and 8 nm, respectively [3]. Ansoft HFSS finite element method is used to simulate the antenna structure. The spectral response of the antenna is shown in Fig. 5. The antenna has a broadband response in most part of the 300-750 nm wavelength range with the highest field enhancement of 26 times at the 650 nm. The near- and far-field patterns of the plane wave incident at 652 nm are also simulated using HFSS, as shown in Fig. 6. Figure 7 shows the E-field steady state pattern of the bowtie antenna structure at the different frequencies. It displays the field enhancement at the antenna gap range at these frequencies.

To further test the feasibility of the antenna solar cell structure, we simulated antenna arrays on the silicon substrate. Fig. 8 shows a 5 × 5 array with the plane wave incident at 652 nm wavelength. The antenna array period in x and y direction are both of 230 nm. The dimension of the antenna, the silicon substrate and the ground plane are the same as the single antenna simulated above. The field enhancement is 26 times, which is the same as the single antenna case. From this simulation result, we can see the antenna array structure can significantly increase the field collection efficiency of the solar cell.

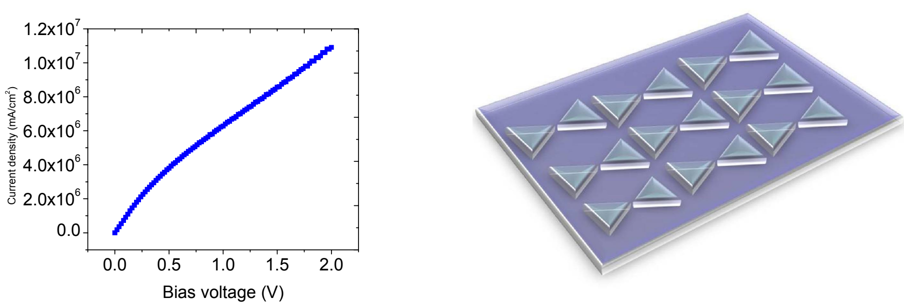

Fig. 4. Current intensity v.s. bias voltage of the p-n-p HPT and the nano-antenna structure for solar cell applications

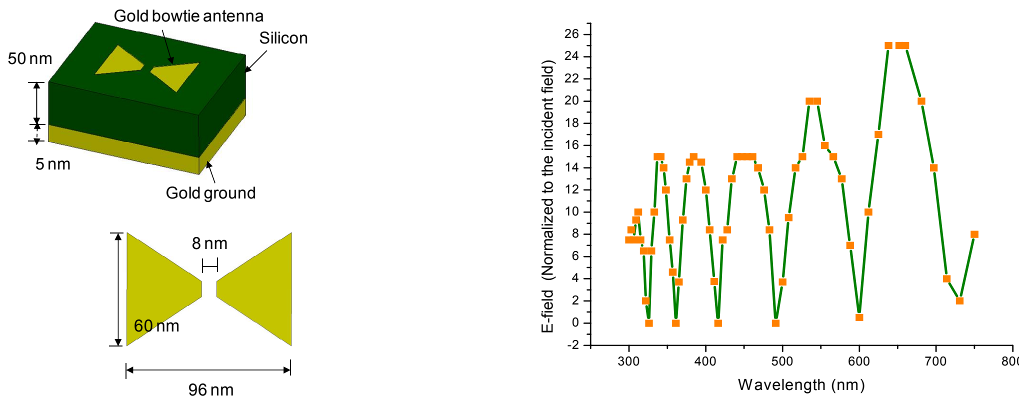

Fig. 5. Nano-antenna structure for solar cell application and its spectral-response

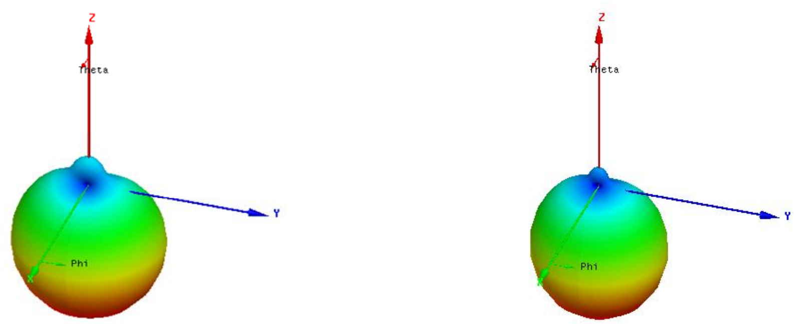

Fig.6. Near- and far- field pattern of the antenna solar cell at 652 nm, simulated using HFSS.

4. CONCLUSION

In this paper, the characteristics of InGaAsSb/alGaAsSb phototransistors were presented. The new devices were grown using the MBE technique and are sensitive in the 1.0-2.2- µm wavelength range. In addition, wide band bowtie antennas are designed to increase the efficiency of the solar cell. Preliminary simulation results show the field enhancement in the gap area can reach up to 29 times that of the incident plane wave.

REFERENCES

[1] T. F. Refaat, M. N. Abedin, O. V. Sulima, S. Ismail, and U. N. Singh, " AlGaAsSb/InGaAsSb phototransistors for 2-µm remote sensing applications," *Optical Engineering*, **43(7)** 1647-1650 (2004).

[2] H. Shao, W. Li, *et al.*, "Room-temperature p-n-p AlGaAsSb-InGaAsSb heterojunction phototransistors with cutoff wavelength at 2.5 µm," IEEE PTL. **18(20)**, 2325-2337 (2006).

[3] N. Yu, E. Cubukcu, F. Capasso *et al.,* " Bowtie plasmonic quantum cascade laser antenna," *Optics Express* **15(20)** 13272-13281 (2007)

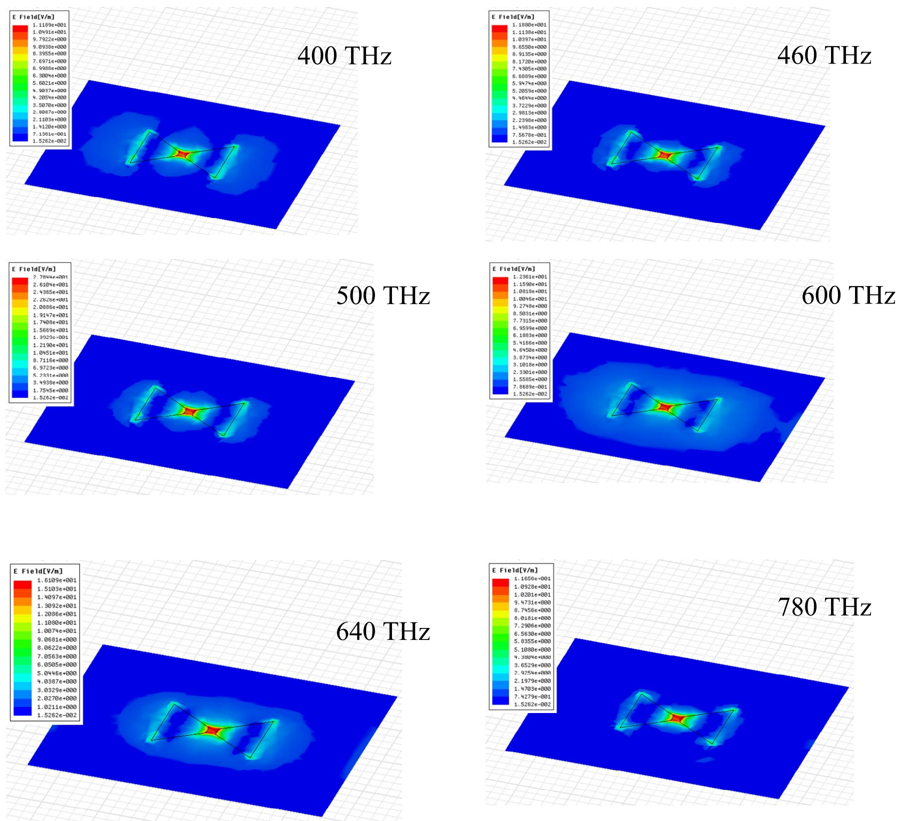

Fig. 7. E-field distribution of the antenna solar cell at different frequencies, simulated using HFSS

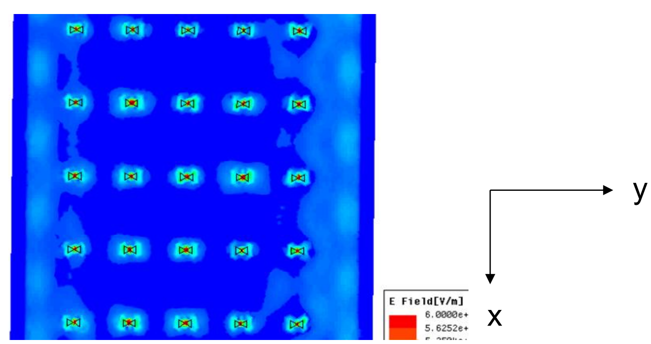

Fig. 8. E-field distribution of the 5 × 5 antenna array, simulated using HFSS